Ultrafast photodynamics of pyrazine in the vacuum ultraviolet region studied by time-resolved photoelectron imaging using 7.8-eV pulses

Takuya Horio, Yoshi-ichi Suzuki, and Toshinori Suzuki

Citation: The Journal of Chemical Physics **145**, 044307 (2016); doi: 10.1063/1.4955298
View online: https://doi.org/10.1063/1.4955298
View Table of Contents: http://aip.scitation.org/toc/jcp/145/4
Published by the American Institute of Physics

Ultrafast photodynamics of pyrazine in the vacuum ultraviolet region studied by time-resolved photoelectron imaging using 7.8-eV pulses

Takuya Horio, Yoshi-ichi Suzuki,[a] and Toshinori Suzuki[b]
Department of Chemistry, Graduate School of Science, Kyoto University, Kitashirakawa Oiwake-cho, Sakyo-Ku, Kyoto 606-8502, Japan

(Received 1 April 2016; accepted 20 May 2016; published online 25 July 2016)

The ultrafast electronic dynamics of pyrazine ($C_4N_2H_4$) were studied by time-resolved photoelectron imaging (TRPEI) using the third (3ω, 4.7 eV) and fifth harmonics (5ω, 7.8 eV) of a femtosecond Ti:sapphire laser (ω). Although the photoionization signals due to the 5ω − 3ω and 3ω − 5ω pulse sequences overlapped near the time origin, we have successfully extracted their individual TRPEI signals using least squares fitting of the observed electron kinetic energy distributions. When the 5ω pulses preceded the 3ω pulses, the 5ω pulses predominantly excited the S_4 ($\pi\pi^*$, $^1B_{1u}$+$^1B_{2u}$) state. The photoionization signal from the S_4 state generated by the time-delayed 3ω pulses was dominated by the $D_3(^2B_{2g}) \leftarrow S_4$ photoionization process and exhibited a broad electron kinetic energy distribution, which rapidly downshifted in energy within 100 fs. Also observed were the photoionization signals for the $3s$, $3p_z$, and $3p_y$ members of the Rydberg series converging to $D_0(^2A_g)$. The Rydberg signals appeared immediately within our instrumental time resolution of 27 fs, indicating that these states are directly photoexcited from the ground state or populated from S_4 within 27 fs. The $3s$, $3p_z$, and $3p_y$ states exhibited single exponential decay with lifetimes of 94 ± 2, 89 ± 2, and 58 ± 1 fs, respectively. With the reverse pulse sequence of 3ω − 5ω, the ultrafast internal conversion (IC) from $S_2(\pi\pi^*)$ to $S_1(n\pi^*)$ was observed. The decay associated spectrum of S_2 exhibited multiple bands ascribed to D_0, D_1, and D_3, in agreement with the 3ω-pump and 6ω-probe experiment described in our preceding paper [T. Horio *et al.*, J. Chem. Phys. **145**, 044306 (2016)]. The electron kinetic energy and angular distributions from S_1 populated by IC from S_2 are also discussed. *Published by AIP Publishing.* [http://dx.doi.org/10.1063/1.4955298]

I. INTRODUCTION

In our preceding paper,[30] we have discussed time-resolved photoelectron imaging (TRPEI) using the 6th harmonic (6ω; 9.3 eV) of a femtosecond Ti:sapphire laser (ω) to fully probe cascaded radiationless transitions from an excited state. In this paper, we present TRPEI using the 5th harmonic (5ω; 7.8 eV) and discuss its characteristics in the studies of photophysics and photochemistry of molecules.

Figure 1 shows a photoabsorption spectrum of pyrazine ($C_4N_2H_4$, D_{2h}) vapor in the region from 4.5 to 12 eV.[1] As seen here, vacuum UV (VUV) photoabsorption spectra of large molecules are highly congested, due to the large number of transitions to the Rydberg (R) and higher-valence states (S_i). However, it is noted that the broadness of the absorption bands is also indicative of the ultrafast dynamics of these states. The absorption cross sections are quite large in the VUV region; for example, the transition(s) to $S_4(\pi\pi^*)$, which corresponds to the $^1E_{1u}$ state of benzene (D_{6h}),[2] has a cross section as large as 120 Mb. A number of sharp peaks around the S_4 band are transitions to low-lying Rydberg states and associated vibrational structures. Because of such complex spectral features in the VUV region, photoexcitation in this region is expected to initiate dynamics involving the strongly coupled valence and Rydberg states.

TRPEI is highly useful for studying complex ultrafast electronic dynamics.[3] The method enables straightforward distinction of Rydberg states from higher-valence excited states, because photoionization from a Rydberg state provides a characteristic sharp photoelectron kinetic energy distribution (PKED), and valence states usually exhibit much broader PKEDs. Time-dependent photoelectron angular distributions (PADs) are also of great assistance for resolving these states, because Rydberg states generally exhibit strong photoemission anisotropy whereas valence states do not. While TRPEI studies in the VUV region have been scarce owing to the difficulty in generating ultrashort VUV pulses, filamentation four-wave mixing enables the generation of sub-20 fs VUV pulses using a relatively simple apparatus[4,5] and has changed this situation.

In our previous study on VUV-TRPEI of furan (C_4OH_4, C_{2v}) using the 4th harmonic (4ω; 6.3 eV) and 5ω pulses,[6] a higher-valence $^1A_1(\pi\pi^*)$ state was populated by the 5ω pulses, and an ultrafast (<100 fs) structural deformation on the $^1A_1(\pi\pi^*)$ state was observed from the time-evolution of the PKEDs measured using the time-delayed 4ω. One of the key findings was that low-lying Rydberg states, $^1B_1(2b_1 \rightarrow 3s)$, $^1B_1(1a_2 \rightarrow 3p_y)$, and $^1B_2(1a_2 \rightarrow 3p_x)$, were populated via the $^1A_1(\pi\pi^*)$ state, suggesting the existence of conical intersections (CIs) between the $^1A_1(\pi\pi^*)$ state and

[a]Present address: Faculty of Pharmaceutical Science, Health Sciences University of Hokkaido, Ishikari-Tobetsu, Hokkaido 061-0293, Japan.
[b]Author to whom correspondence should be addressed. Electronic mail: suzuki@kuchem.kyoto-u.ac.jp

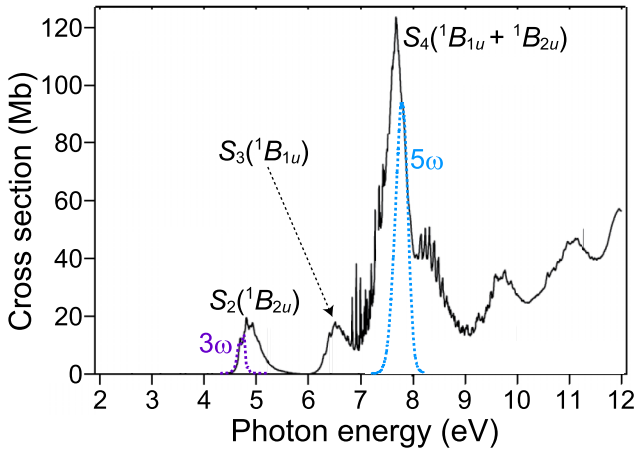

FIG. 1. Photoabsorption spectrum of pyrazine vapor from 4.5 to 12 eV overlaid with the spectra of the third (3ω, 4.7 eV) and fifth harmonics (5ω, 7.8 eV) pulses of a femtosecond Ti:sapphire laser (ω) used in this study. The photoabsorption spectrum was adapted with permission from M. Stener *et al.*, J. Phys. B: At., Mol. Opt. **44**, 075203 (2011). Copyright 2011 IOP Publishing Ltd.

the low-lying Rydberg states along the structural deformation coordinate.

In the present paper, we report similar VUV-TRPEI of pyrazine using 5ω-pump and 3rd-harmonic (3ω; 4.7 eV) probe pulses, in order to further investigate the photophysics of large molecules in the VUV region. As shown in Fig. 1, 5ω and 3ω are, respectively, resonant with transitions to S_4 and Rydberg states and with the $S_2(\pi\pi^*, {}^1B_{2u}) \leftarrow S_0({}^1A_g)$ transition. As mentioned in our preceding paper,[30] the $S_2(\pi\pi^*) \rightarrow S_1(n\pi^*)$ internal conversion (IC) in pyrazine is a benchmark system to study ultrafast non-adiabatic transitions via a CI of potential energy surfaces (PESs), which motivated us to employ 3ω in combination with 5ω in the present study; the reverse pulse sequence, i.e., a 3ω-pump and 5ω-probe scheme, enabled us to explore this benchmark IC process. As reported in the preceding paper,[30] the ultrafast cascaded radiationless transitions from $S_2(\pi\pi^*)$ of pyrazine were fully observed by TRPEI using 6ω. The TRPEI experiment on pyrazine using 5ω presented here was performed prior to our 6ω experiment, and the results motivated us to extend it to 6ω. Both the 5ω − 3ω and 3ω − 5ω pulse sequences create photoionization signals in the same energy region, and the photoionization signals overlap with each other around the time-origin. We will describe how these signals are deconvoluted to extract individual signals, discuss the characteristics of TRPEI using 5ω, and compare the results with those of TRPEI using 6ω.

II. EXPERIMENTAL METHOD

The light source, photoelectron imaging apparatus, data acquisition system, and image analysis procedures used in this study were identical to those described in the preceding paper.[30] The pump-probe setup using 3ω and 5ω pulses was realized by replacing the dielectric mirrors designed for 6ω used in the preceding study with those for 5ω. The pulse energies of 3ω and 5ω on the molecular beam were estimated to be ~500 nJ/pulse and ~50 nJ/pulse, respectively. The cross-correlation function between the 3ω and 5ω pulses was measured using non-resonant (1 + 1′) multiphoton ionization of xenon, and it was found to be a single Gaussian with a full width at half maximum (FWHM) of 27 fs. Figure 2 shows a schematic diagram of the pump-probe scheme employed in this study. For positive delay times, 5ω preceded 3ω, so that 5ω and 3ω acted as the pump and probe pulses, respectively, and vice versa for negative delay times. Photoelectron images were measured as a function of the pump-probe delay time from −162 to 183 fs at 5 fs intervals. Each image was integrated for 13 s, and the measurement was repeated 30 times. The 30 images at each delay time were combined, from which the original three-dimensional (3D) scattering distributions were reconstructed using *p*-BASEX.[7] Time-independent background images due to one-color photoionization by each pulse were subtracted prior to the reconstruction. PKE calibration was performed using one-color three-photon ionization of xenon with 3ω pulses.

We employed (1 + 1′) resonantly enhanced multiphoton ionization (REMPI) using linearly polarized pump and probe pulses with parallel polarizations. Therefore, the time-dependent photoionization cross sections, $I(E,\theta,t)$, can be expressed as

$$I(E,\theta,t) = \frac{\sigma(E,t)}{4\pi}[1 + \beta_2(E,t)P_2(\cos\theta) + \beta_4(E,t)P_4(\cos\theta)], \quad (1)$$

where E, θ, and t, respectively, denote the PKE, photoelectron ejection angle with respect to the laser polarization and pump-probe delay time, and $P_n(x)$ is an nth order Legendre polynomial. In addition, $\sigma(E,t)$ denotes the PKEDs, and the coefficients, β_2 and β_4, are photoelectron anisotropy parameters that depend on both E and t.

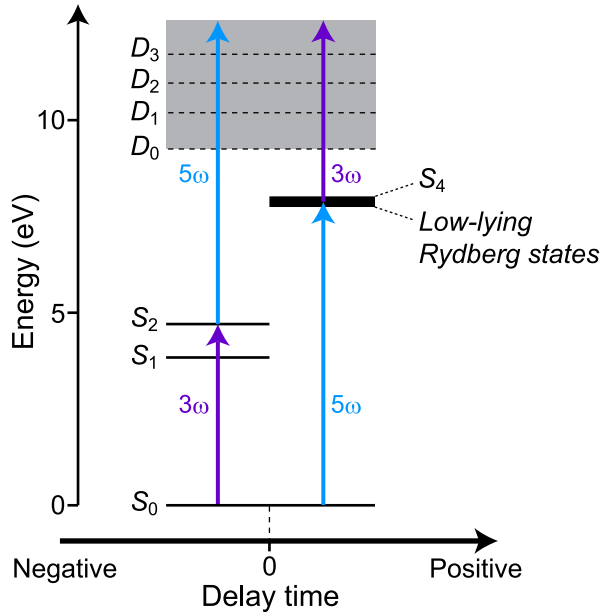

FIG. 2. Schematic diagram of the pump-probe scheme employed in this study.

III. RESULTS AND DISCUSSION

Figure 3 shows two-dimensional (2D) slices through the 3D photoelectron scattering distributions at delay times of −22 and 38 fs, which highlights that entirely different distributions occur between the 5ω − 3ω and 3ω − 5ω pulse sequences.

The total photoelectron yield is presented in Fig. 4(a) as a function of the delay time between the 3ω and 5ω pulses. In the plot, the time-independent background signals due to one-color photoionizations have been subtracted so that zero intensity corresponds to the signal level of the time-independent one-color background. Time-dependent photoionization signals can be seen for both the 5ω − 3ω and 3ω − 5ω pulse sequences. In Subsections III A and III B, the results observed for these pulse sequences are discussed separately.

A. 5ω-pump and 3ω-probe pulse sequence

Figure 4(b) shows a 2D time-energy map of PKEDs, namely, $\sigma(E,t)$ in Eq. (1). The map exhibits a short-lived component with a broad energy distribution in the PKE region lower than ∼1 eV, and three long-lived components in the PKE region between 1.4 and 3 eV, whose characteristic feature is their narrow bandwidth. As discussed in Section I, the broad and sharp components of $\sigma(E,t)$ can be immediately assigned to photoionization from valence-excited and Rydberg states, respectively. These assignments are further supported by examining the 2D map of $\beta_2(E,t)$ presented in Fig. 4(d). It is clear from the figure that $\beta_2(E,t)$ is strongly dependent on E: the β_2 values in the PKE regions where the three sharp components (Rydberg states) were observed are quite high (0.8–1.1), as denoted using red, while the broad component from the valence state exhibits much lower β_2 values (0.0–0.4). These are well-established fingerprints for photoionization processes from Rydberg and valence states. The results clearly demonstrate that 2D mapping of $\sigma(E,t)$ and $\beta_2(E,t)$ by TRPEI is effective for discerning the electronic characters of non-stationary states in the VUV region.

Let us first examine the broad PKED in Fig. 4(b). Based on Fig. 1, this broad component is unambiguously assigned to photoionization from the $S_4(\pi\pi^*)$ state created by the 5ω pulses. Theoretical investigations on the electronic excited states of pyrazine[8–11] showed that the electronic character

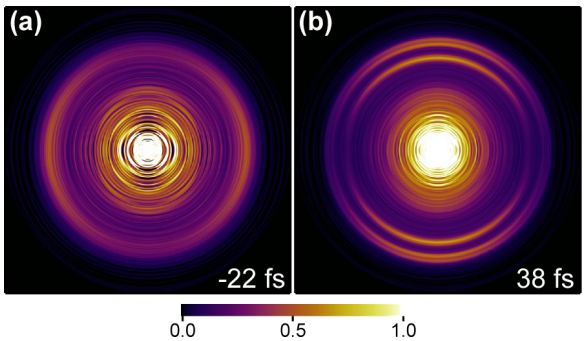

FIG. 3. 2D slices of the 3D photoelectron scattering distributions obtained at the delay times of (a) −22 and (b) 38 fs.

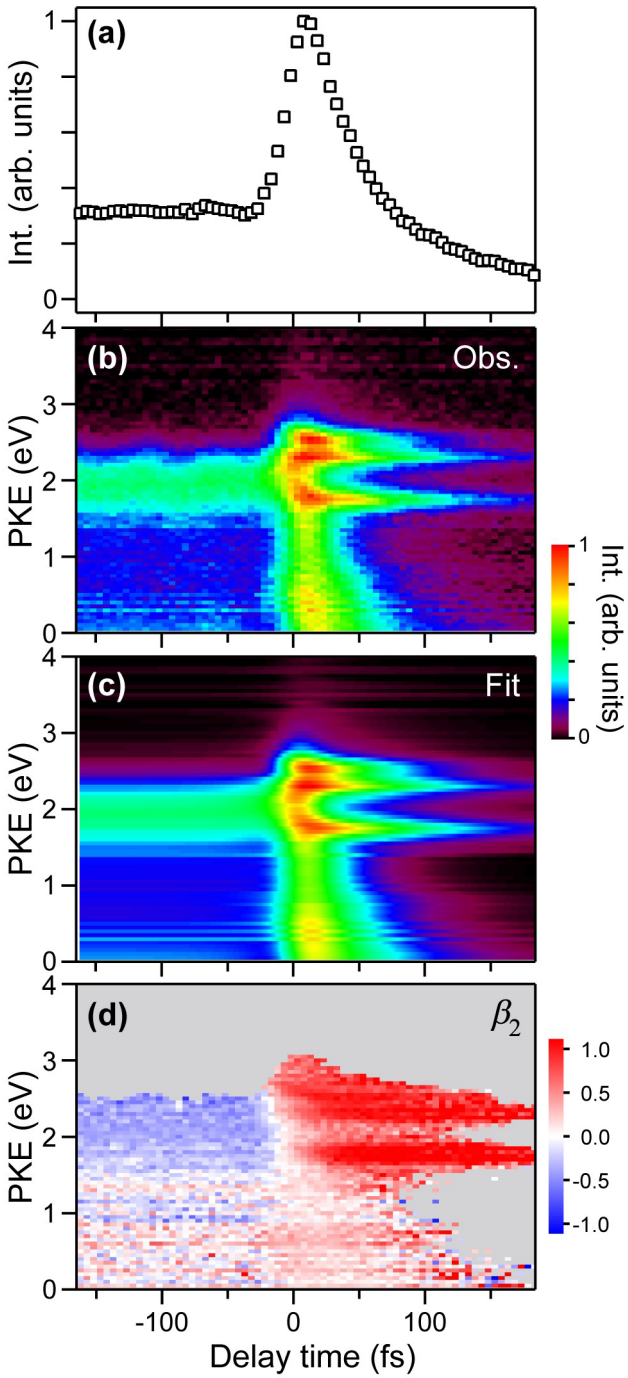

FIG. 4. (a) Total photoelectron yield as a function of the delay time between the 3ω and 5ω pulses. For positive delay times, 5ω preceded 3ω, and vice versa for negative delay times. (b) Observed and (c) fitting result of time-dependent photoelectron kinetic energy distributions. (d) Time-dependent photoelectron anisotropy parameter, β_2. The β_2 values are displayed only in the regions where the normalized photoelectron intensities in (b) are greater than 0.1.

of the $S_4(\pi\pi^*)$ state can be described as $^1B_{1u} + {}^1B_{2u}$, as they are almost degenerate. The former ($^1B_{1u}$) has a leading configuration of $(1b_{2g})^{-1}(2b_{3u})^{+1}$, while the latter ($^1B_{2u}$) has a leading configuration of $(1b_{2g})^{-1}(1a_u)^{+1}$. Since $D_3(^2B_{2g})$ has a single leading configuration of $(1b_{2g})^{-1}$,[12–14] both of the photoionization processes, $(1b_{2g})^{-1} \leftarrow (1b_{2g})^{-1}(2b_{3u})^{+1}$ and $(1b_{2g})^{-1} \leftarrow (1b_{2g})^{-1}(1a_u)^{+1}$, are allowed: an electron in the $2b_{3u}$ or the $1a_u$ orbital is ejected by the 3ω pulses

without changing the electronic configuration of the ion core, $(1b_{2g})^{-1}$. Thus, photoionization from S_4 by the 3ω probe pulses predominantly yields D_3. In the present study, the total photon energy of 3ω and 5ω is 12.5 eV, indicating that the four cationic states $D_0(^2A_g)$, $D_1(^2B_{1g})$, $D_2(^2B_{1u})$, and $D_3(^2B_{2g})$ are energetically accessible. The largest possible PKEs, E_i^{max}, were estimated for each cationic state, D_i, from high-resolution photoelectron spectra[15,16] in the literature. The estimated values for E_0^{max}, E_1^{max}, E_2^{max}, and E_3^{max} are 3.21, 2.33, 1.57, and 0.84 eV, respectively, suggesting that the broad component in the lower energy region (<1 eV) should be assigned to $D_3 \leftarrow S_4$.

As can be seen in Fig. 4(b), the S_4 PKED exhibits a progressive energy shift towards zero PKE, indicating wavepacket motion on the S_4 PES. When the wavepacket moves away from the Franck-Condon region, higher photon energy is required for photoionization: The photon energy of the 3ω pulse (4.7 eV) is insufficient to induce ionization from the entire S_4 PES, leading to diminished photoelectron intensity. Thus, the photoelectron intensity does not represent the S_4 population accurately. The wavepacket motion can be related to some ultrafast structural deformation occurring on the S_4 state, although the deformation coordinate is unclear at this point.

Next, we discuss the Rydberg states observed as three sharp bands in the PKE region from 1.4 to 3.0 eV. For a closer examination of the three components, Fig. 5 presents PKEDs obtained at 28, 43, 58, and 118 fs. The three dotted lines in the figure indicate their peak positions. The term values of the observed Rydberg states, T, can be calculated using the following relation:

$$T = PKE + IE - \hbar\omega_{probe}, \quad (2)$$

where IE and $\hbar\omega_{probe}$ are the ionization energy of pyrazine for $D_0(n^{-1},{}^2A_g)$ (9.288 eV)[16] and the probe photon energy, respectively. The term values thus calculated are summarized in Table I.

Walker and Palmer[9] estimated the term values of the $3p_x(n^{-1})$, $3p_y(n^{-1})$, and $3p_z(n^{-1})$ Rydberg states of pyrazine to be 6.75, 7.07, and 6.84 eV, respectively, using VUV photoabsorption spectroscopy, electron energy loss spectroscopy, and *ab initio* multireference configuration interaction calculations. In our previous study using picosecond (2 + 1) REMPI spectroscopy,[16] we estimated the term value of the $3s(n^{-1})$ state of pyrazine to be 50 844(8) cm^{-1} (6.30 eV), which was

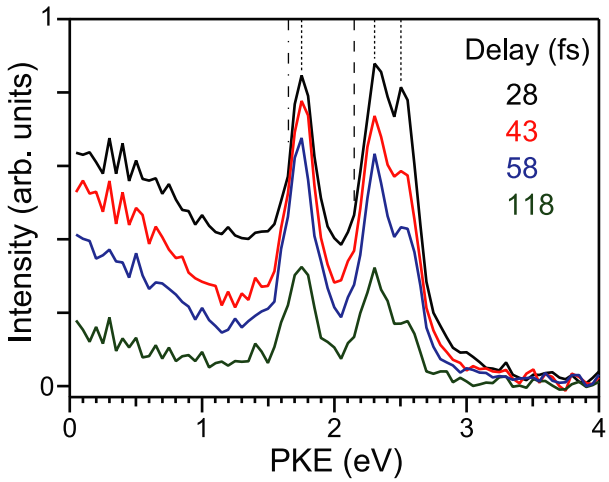

FIG. 5. PKEDs obtained at 28, 43, 58, and 118 fs. Dotted lines indicate the peak positions for $^1R(3s)$, $^1R(3p_z)$, and $^1R(3p_y)$ (see the text). The expected PKEs for the $^1R(3p_x)$ and $3s(\pi^{-1})$ Rydberg states are shown using dashed and dashed-dotted lines, respectively.

in fair agreement with the estimated values of 50 830 cm^{-1} by Turner *et al.*[17] and 50 835 cm^{-1} by Dion and Bernstein[18] using nanosecond (2 + 1) REMPI spectroscopy. Using femtosecond (2 + 1) REMPI spectroscopy, Song *et al.*[19] measured the term values of $3p_y(n^{-1})$ and $3p_z(n^{-1})$ as 56 800 cm^{-1} (7.04 eV) and 55 000 cm^{-1} (6.82 eV), respectively. Based on a comparison with the results of these previous studies, the three peaks shown in Fig. 5 are assigned to $3s(n^{-1})$, $3p_z(n^{-1})$, and $3p_y(n^{-1})$ in order of increasing PKE. No signal was observed for the $3p_x(n^{-1})$ Rydberg state, for which the expected PKE is 2.16 eV, as indicated by the dashed line in Fig. 5. In a previous study,[19] we identified the $3s(\pi^{-1})$ Rydberg state with the term value of 7.130 eV. Based on this term value and the ionization energy of D_1 (π^{-1}), 10.169 eV, its signal for the current pump-probe scheme is expected at 1.657 eV, as indicated by the dashed-dotted line in Fig. 5. However, no noticeable signal of the $3s(\pi^{-1})$ Rydberg state was identified. Hereafter, we denote the $3s(n^{-1})$, $3p_x(n^{-1})$, $3p_y(n^{-1})$, and $3p_z(n^{-1})$ Rydberg states as $^1R(3s)$, $^1R(3p_x)$, $^1R(3p_y)$, and $^1R(3p_z)$, as in the preceding paper.[30]

To evaluate the lifetimes of the $^1R(3s)$, $^1R(3p_z)$, and $^1R(3p_y)$ states, we extracted their photoelectron signals in the PKE regions of 1.70–1.80, 2.25–2.35, and 2.45–2.55 eV

TABLE I. Summary of the observed Rydberg states. Term values from the literature are also shown. Lifetimes were obtained using Eq. (3).

	Term values (eV)					
Position (eV)	This work	References 16–18	Reference 9	Reference 19	Assignment[a]	Lifetime (fs)[b]
2.50	7.09	...	7.07 (7.20)[c]	7.04	$3p_y(n^{-1})$, $^1B_{2u}$	58 ± 1
2.30	6.89	...	6.84 (6.94)[c]	6.82	$3p_z(n^{-1})$, $^1B_{1u}$	89 ± 2
1.75	6.34	6.30	(6.11)[c]	6.29	$3s(n^{-1})$, ^1A_g	94 ± 2

[a]The z-axis is defined along the C_2 axis through the two nitrogen atoms, and the x-axis is perpendicular to the molecular plane.
[b]Note that these lifetimes were obtained for $3p_y(n^{-1})$, $3p_z(n^{-1})$, and $3s(n^{-1})$ Rydberg states with internal energies of 0.71, 0.91, and 1.46 eV, respectively.
[c]The values in parentheses were obtained by *ab initio* multireference configuration interaction calculations.

and performed least squares fitting using the following formula:

$$I(t) = \left[C_R \exp(-\frac{t}{\tau_R}) + C_{S_4} \exp(-\frac{t}{\tau_{S_4}}) + C_{S_2} \exp\left(\frac{t}{\tau_{S_2}}\right) + C_{S_1}\left(1 - \exp\left(\frac{t}{\tau_{S_2}}\right)\right)\right] \otimes g(t), \quad (3)$$

where $g(t)$ is the pump-probe cross-correlation function. C_R/C_{S_4} and τ_R/τ_{S_4}, respectively, denote the amplitudes of the Rydberg/S_4 component and their time constants. The ultrafast IC process from S_2 to S_1 observed at negative time delays was also taken into account. The S_2 lifetime is 22 fs,[20] while S_1 populated via IC from S_2 is rather long-lived. Therefore, the photoionization signal from S_1 yields the plateau visible in Fig. 4(a). In the least squares fitting, we fixed the S_2 lifetime, τ_{S2}, to be 22 fs.

The extracted photoionization signals and the results of the least squares fitting are presented in Fig. 6. The least squares fitting well reproduces the transient signals for both positive and negative time delays. The lifetimes of $^1R(3s)$, $^1R(3p_z)$, and $^1R(3p_y)$ are summarized in Table I. Note that our excitation pulses create $^1R(3s)$, $^1R(3p_z)$, and $^1R(3p_y)$ with excess energies of 1.46, 0.91, and 0.71 eV, respectively; therefore, lifetimes at their origin (zero vibrational level in each state) are expected to be longer than the values observed in the present study. In fact, the lifetime for $^1R(3s)$ at the origin has been estimated to be 300 fs by Dion and Bernstein.[18]

In our previous TRPEI study on furan using 4ω and 5ω pulses,[6] a higher-valence $^1A_1(\pi\pi^*)$ state was populated by the 5ω pump pulses, and its ultrafast dynamics were clearly observed by one-photon ionization using the 4ω probe pulses. The 2D map of the observed PKEDs was dominated by multiple photoionization signals from $^1A_1(\pi\pi^*)$ into D_0, D_1, and D_2. Three low-lying Rydberg states, $^1B_1(2b_1 \rightarrow 3s)$, $^1B_1(1a_2 \rightarrow 3p_y)$, and $^1B_2(1a_2 \rightarrow 3p_x)$, were also identified in the 2D map. Interestingly, the three Rydberg states appeared with time delays (9, 28, and 18 fs for $^1B_1(2b_1 \rightarrow 3s)$, $^1B_1(1a_2 \rightarrow 3p_y)$, and $^1B_2(1a_2 \rightarrow 3p_x)$, respectively), indicating that they were populated via $^1A_1(\pi\pi^*)$. However, such delayed appearances of the Rydberg states were not identified in the present study. This indicates that the $^1R(3s)$, $^1R(3p_z)$, and $^1R(3p_y)$ Rydberg states observed in the present study were directly populated by the 5ω pump pulses. However, an inconsistency with this interpretation is that the photoionization signals from the Rydberg states seem too strong in comparison with their weak photoabsorption features, as seen in Fig. 1. We therefore conjecture that the $^1R(3s)$, $^1R(3p_z)$, and $^1R(3p_y)$ Rydberg states observed in the present study were populated from the S_4 state in less than our instrumental time resolution (27 fs).

B. 3ω-pump and 5ω-probe pulse sequence

As shown in Fig. 1, 3ω is resonant with the $S_2(\pi\pi^*, {}^1B_{2u}) \leftarrow S_0({}^1A_g)$ transition, so we were able to explore the $S_2(\pi\pi^*, {}^1B_{2u})/S_1(n\pi^*, {}^1B_{3u})$ IC process using a 3ω-pump and 5ω-probe pulse sequence. $S_2(\pi\pi^*, {}^1B_{2u})$ is extremely short-lived (22 fs),[20] because the S_2/S_1 CI occurs in the vicinity of the Franck-Condon region.[21] Consequently, photoionization signal from $S_2(\pi\pi^*, {}^1B_{2u})$ appears only around the time origin of the pump-probe delay time. Compared with our previous study using 4ω (6.3 eV) probe pulses,[20] 5ω (7.8 eV) enables photoionization from much wider regions of the S_2 and S_1 PESs. However, since the 5ω-pump and 3ω-probe pulse sequence creates photoionization signals in the same energy region, the photoionization signals around the time origin become highly congested, as can be seen in Fig. 4(b). In this study, we performed a global fitting by dividing the PKE region into two, as explained below.

As is clear from Figs. 4(b) and 5, no appreciable contributions from any Rydberg states were observed in the PKE regions of 0–1.40 and 3.20–4.00 eV. Thus, we divided the observed 2D map of PKEDs in Fig. 4(b), $I(E,t)$, as follows:

$$I(E,t) = \left[C_{short}(E) \exp(-\frac{t}{\tau_{short(E)}}) + C_{S_2}(E) \exp\left(\frac{t}{\tau_{S_2}}\right) + C_{S_1}(E)\left(1 - \exp\left(\frac{t}{\tau_{S_2}}\right)\right)\right] \otimes g(t),$$
$$(0 < E \leq 1.40 \text{ eV}, 3.20 < E \leq 4.00 \text{ eV}), \quad (4a)$$

$$I(E,t) = \left[C_{short}(E) \exp(-\frac{t}{\tau_{short(E)}}) + C_{long}(E) \exp(-\frac{t}{\tau_{long(E)}}) + C_{S_2}(E) \exp\left(\frac{t}{\tau_{S_2}}\right) + C_{S_1}(E)\left(1 - \exp\left(\frac{t}{\tau_{S_2}}\right)\right)\right] \otimes g(t),$$
$$(1.40 < E \leq 3.20 \text{ eV}). \quad (4b)$$

The short and long-lived components correspond to the S_4 and Rydberg states, respectively. However, it should be noted that $\tau_{short}(E)$ does not provide the lifetime for S_4 because the corresponding PKED clearly varies with the delay time due to the wavepacket motion on the PES, as previously mentioned. In this sense, $\tau_{short}(E)$ is a PKE-dependent phenomenological time constant used to describe the passage of a wavepacket. We extracted the time profiles for each PKE bin with a 0.05-eV width and performed least squares fitting to determine the $C_{S_2}(E)$ and $C_{S_1}(E)$ coefficients, which provide the PKEDs for S_2 and S_1, respectively. The result of the least squares fitting is presented as a 2D

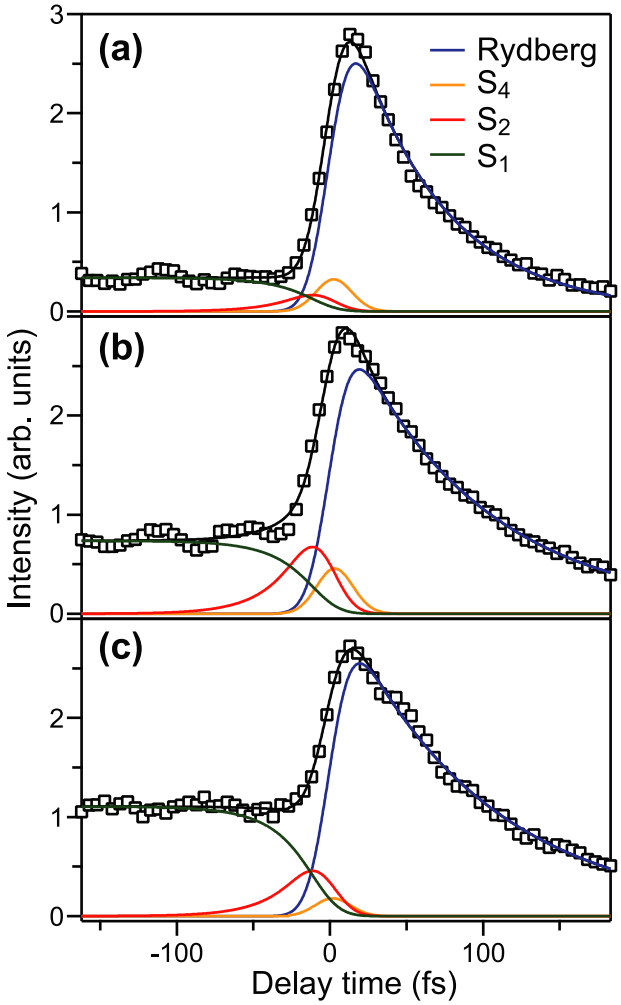

FIG. 6. Photoelectron time profiles obtained for the PKE subsections: (a) 2.45–2.55, (b) 2.25–2.35, and (c) 1.70–1.80 eV. The results of the least squares fittings are also shown with solid lines.

map in Fig. 4(c), which well reproduces the observed 2D map.

The coefficients $C_{S_2}(E)$ and $C_{S_1}(E)$ thus determined are presented in Figs. 7(a) and 7(b), respectively. For $C_{S_2}(E)$, two bands are clearly discernible at ~0.6 and 2.1 eV. The aforementioned values of $E_1^{\max}$ and $E_3^{\max}$ are presented with dotted lines in Fig. 7(a), which indicate that the two bands at ~0.6 and 2.1 eV originate from $D_3 \leftarrow S_2$ and $D_1 \leftarrow S_2$ photoionization processes, respectively. A small intensity on the high energy side (>2.5 eV) of the D_1 band is ascribed to $D_0 \leftarrow S_2$ photoionization.

Figure 8 compares the photoelectron spectra for S_2 obtained by the $3\omega - 5\omega$ (this study) and $3\omega - 6\omega$ (the preceding paper[30]) experiments, which are presented as a function of electron binding energy (eBE). The results are consistent in terms of the band positions. Note that the $D_x \leftarrow S_2$ photoionization process, which was observed in the $3\omega - 6\omega$ experiment (see Figs. 5(a) and 5(b) in the preceding paper[30]), could not be observed in this study due to insufficient photon energy of the 5ω probe pulse. There are two noticeable changes when the probe pulse is switched from 6ω to 5ω. One is the relative intensity of the D_3 band with respect to that of D_1, and the other is the contribution of the D_0 band.

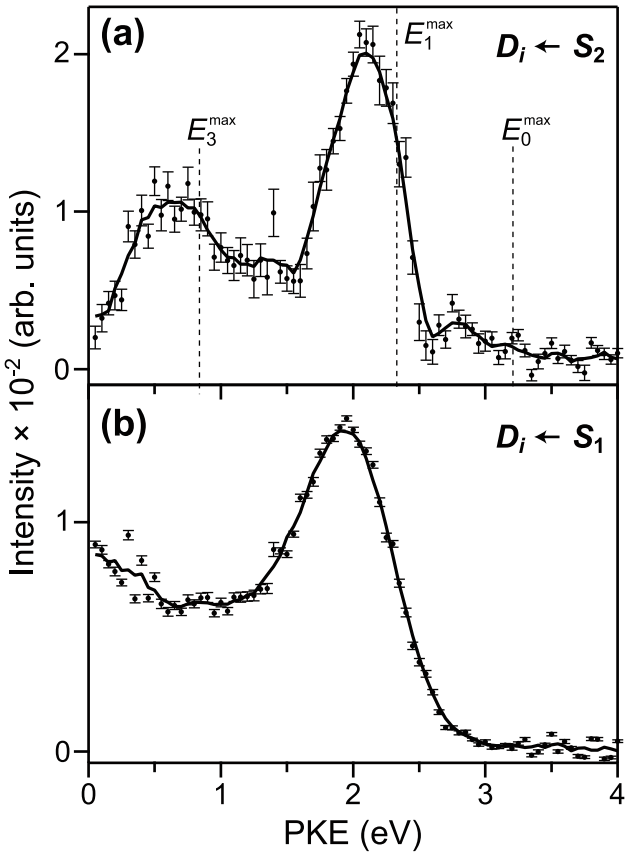

FIG. 7. The coefficients (a) $C_{S2}(E)$ and (b) $C_{S1}(E)$ obtained from the fitting result shown in Fig. 4(c) (filled circles). The error bars correspond to one standard deviation in the fit. The results obtained by 5-points box smoothing (moving average) are presented with solid curves.

These changes suggest that the relative magnitudes of the photoionization cross sections from S_2 into D_0, D_1, and D_3 are PKE-dependent. As for the lower intensity of the D_0 band in the 5ω experiment, it is possible that interference from the intense signals from the $^1R(3p_z)$ and $^1R(3p_y)$ Rydberg states

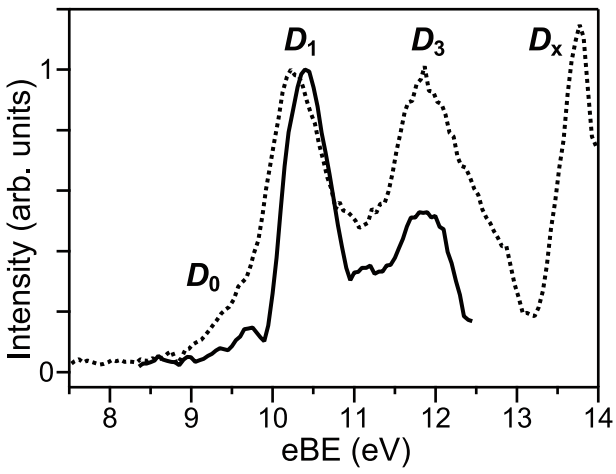

FIG. 8. Comparison of the photoelectron spectra for S_2 obtained by 5ω (solid line) and 6ω (dotted line) probe pulses. The solid line corresponds to the smoothed one shown in Fig. 7(a), while the dotted line was taken from the data shown in Fig. 5(a) of the preceding paper.[30] The vertical scale for each spectrum is normalized to the peak intensity of the D_1 band.

near the time origin led to underestimation in the least squares fitting using Eqs. (4a) and (4b). In addition, this may also be responsible for a small peak shift of the D_1 bands between the two experiments.

Ultrafast IC from S_2 via the S_2/S_1 CI creates a vibrationally hot S_1 state, and $C_{S_1}(E)$ shown in Fig. 7(b) corresponds to the photoelectron spectrum for this state. However, the S_1 photoelectron spectrum can be obtained without relying on the least squares fitting: integration of the observed PKEDs from −162 to −107 fs provides a "time-averaged" S_1 photoelectron spectrum, because the photoionization signal from S_2 is negligible for the corresponding delay times, as can be seen in Fig. 6. The result is presented as a function of eBE in Fig. 9 and is compared with the S_1 spectrum obtained from the 3ω + 6ω experiment. Again, it is clear that the results are consistent with each other, although they deviate slightly at eBEs higher than 11 eV. The band at eBE = ~10.5 eV is due to the $D_0 \leftarrow S_1$ photoionization process. The lowest eBE (adiabatic ionization energy for D_0) is 9.288 eV;[16] however, the observed peak position for D_0 in Fig. 9 is approximately 10.5 eV. The energy difference between S_2 and S_1, 0.86 eV,[22,23] is transformed into the S_1 vibrational energy upon IC, and the vibrational energy is approximately conserved upon $D_0 \leftarrow S_1$ photoionization, which increases the apparent eBE. The observed shift of ~1.2 eV is even larger than 0.86 eV, which is ascribed to the difference between the PESs of S_1 and D_0.

Lastly, we focus on the PKE dependence of the photoelectron angular anisotropy for the $D_0 \leftarrow S_1$ photoionization process. Our successive studies using 4ω, 5ω, and 6ω probe pulses enabled us to measure $\beta_2(E)$ for the $D_0 \leftarrow S_1$ process over a wide energy range of 0–4 eV, as presented in Fig. 10. The $\beta_2(E)$ values were obtained in the PKE regions where the photoelectron bands corresponding to $D_0 \leftarrow S_1$ photoionization were observed: 0.2–1.0, 1.5–2.5, and 3.0–4.0 eV for the 4ω, 5ω, and 6ω probe pulses, respectively. The β_2 values were time-averaged over the pump-probe delays

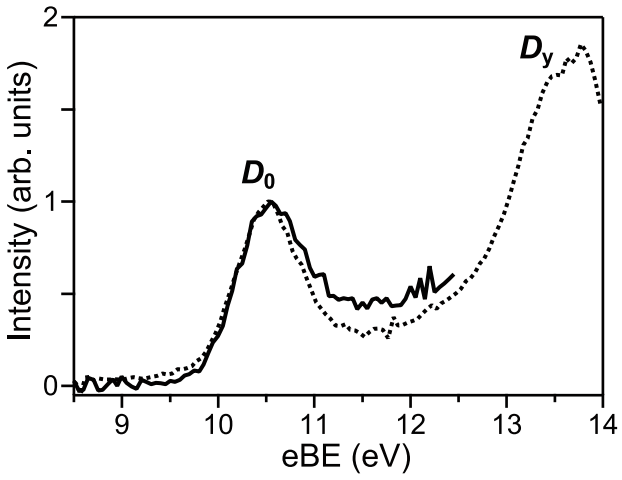

FIG. 9. Comparison of the photoelectron spectra for vibrationally hot S_1 obtained by 5ω (solid line) and 6ω (dotted line) probe pulses. The solid line is obtained by integration of the PKEDs presented in Fig. 4(b) from −162 to −107 fs, while the dotted line is obtained by the integration of the PKEDs presented in Fig. 6(a) of the preceding paper from 108 to 168 fs.[30]

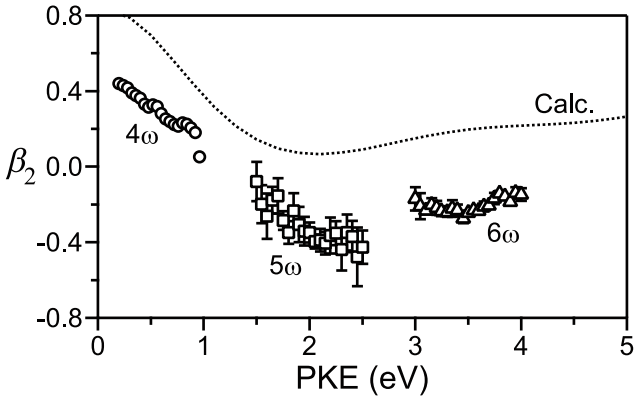

FIG. 10. $\beta_2(E)$ for $D_0 \leftarrow S_1$ photoionization measured by 4ω (circles), 5ω (squares), and 6ω (triangles) probe pulses. The pump pulse was 3ω for each experiment. The experimental data for a 4ω probe were taken from our previous study,[26] while those for 5ω and 6ω probes were obtained in the present and preceding studies,[30] respectively. The β_2 values were time-averaged over the pump-probe delays of 103–393, 107–162, and 108–168, fs for 3ω − 4ω, 3ω − 5ω, and 3ω − 6ω experiments, respectively. Our theoretical prediction from the previous study[24] is shown with a dotted line.

of 103–393, 107–162, and 108–168 fs for the 3ω − 4ω, 3ω − 5ω, and 3ω − 6ω experiments, respectively.

As shown in Fig. 10, β_2 is around 0.4 near the threshold and exhibits a strong negative dependence on PKE from 0 to 2 eV: the dependence is approximately linear with a slope of around −0.4 eV^{-1}. The β_2 value reaches around −0.4 at 2 eV and then gradually increases with PKE. In a previous theoretical study of the photoelectron angular anisotropy for pyrazine,[24] we calculated $\beta_2(E)$ for the $D_0 \leftarrow S_1$ process using the continuum multiple scattering Xα (CMXα) approximation. In the present (1 + 1′) REMPI scheme, the molecular axis is aligned by a 3ω fs pulse via the y-transition dipole (S_2, $^1B_{2u}$), and S_1 is created from S_2 by ultrafast IC (~22 fs) without changing the molecular axis alignment, which was taken into account in the calculation. Small variations in the molecular axis alignment due to rotational dephasing were neglected in the calculation since the observation time window is narrow (<200 fs), and the calculation was performed with both S_0 and S_1 equilibrium geometries. Further details regarding the calculations may be found in the literature.[24]

The $\beta_2(E)$ calculated for $D_0 \leftarrow S_1$ photoionization using the S_1 equilibrium geometry is presented as the dotted line in Fig. 10. Our theoretical prediction qualitatively reproduces the observed PKE dependence of β_2: the observed minimum for $\beta_2(E)$ is around 2 eV, which is in excellent agreement with our prediction. A partial wave analysis carried out in the previous study[24] showed that the pronounced variation of $\beta_2(E)$ is ascribed to a shape resonance, in which a photoelectron is temporarily trapped by a potential barrier due to a centrifugal force. A similar significant variation of $\beta_2(E)$ due to a shape resonance has recently been reported by Staniforth *et al.*,[25] in which the $S_1(\pi\pi^*)$ states of difluorobenzene isomers with ortho, meta, and para substitutions were ionized by one-photon ionizations using nanosecond UV and VUV pulses. They measured $\beta_2(E)$ in the PKE region from 0 to 3.5 eV and found that for each isomer, $\beta_2(E)$ varied strongly due to a shape resonance: $\beta_2(E)$ rapidly decreases with increasing

PKE from the ionization threshold and then starts to increase at PKEs of less than 1 eV, which was qualitatively reproduced by their CMXα calculations.

IV. CONCLUSION

We studied the ultrafast electronic dynamics of pyrazine using TRPEI with 3ω and 5ω femtosecond pulses. Previously, we performed TRPEI of this molecule using a VUV free-electron laser (Spring-8 Compact SASE Source, SCSS) synchronized with a tunable femtosecond UV laser,[27] in which the wavelengths of pump and probe pulses were, respectively, set at 260 and 161 nm. The 161-nm (7.7 eV) VUV pulse should have created S_4 and low-lying Rydberg states; however, the low repetition rate (10 Hz) of the SCSS and the limited beam time prevented us from carrying out a detailed study on these states. The present study using 3ω and 5ω generated from our 1 kHz light source enabled direct observation of the S_4 and $^1R(3s)$, $^1R(3p_z)$, and $^1R(3p_y)$ Rydberg states with a high time-resolution of 27 fs. Time-energy mapping of $\sigma(E,t)$ and $\beta_2(E,t)$ enabled us to discern complex electronic dynamics in the VUV region, where a large number of electronic states exist.

Using a 3ω-pump and 5ω-probe pulse sequence, we investigated ultrafast $S_2(\pi\pi^*) \rightarrow S_1(n\pi^*)$ IC dynamics. While the strong signal due to the 5ω-pump and 3ω-probe pulse sequence interfered with observation of the short-lived S_2 state, we were able to successfully extract the photoionization signal (decay associated spectrum) from S_2, which is consistent with the result obtained by TRPEI using 3ω-pump and 6ω-probe pulses. The PKE dependence of the photoelectron angular anisotropy for the $D_0 \leftarrow S_1$ photoionization process was found to be consistent with our previous theoretical calculations.[24]

As demonstrated in the preceding[30] and present papers, a fs-VUV laser is a highly useful light source not only for studying the ultrafast electronic dynamics of higher-valence and Rydberg states but also for observing the entire photophysical and photochemical processes using TRPES or TRPEI. Whenever it is possible, it is advantageous to set the probe wavelength to be non-resonant with any strong photoabsorption band of a target molecule. In this sense, wavelength tunability of the probe laser is useful. In our previous study,[28] we employed collinear filamentation four-wave mixing using a tunable near-infrared light from a non-collinear optical parametric amplifier and the 2nd harmonic of a Ti:sapphire laser. Ghotbi *et al.*[29] have also developed tunable fs-VUV pulses in the wavelength range from 151 to 146 nm (8.2–8.5 eV) using non-collinear four-wave mixing. On the other hand, the key advantage of the light source with fixed photon energies employed in the preceding[30] and present paper is its simplicity and ease of implementation.

[1] M. Stener, P. Decleva, D. M. P. Holland, and D. A. Shaw, J. Phys. B: At., Mol. Opt. **44**, 075203 (2011).
[2] A. Bolovinos, P. Tsekeris, J. Philis, E. Pantos, and G. Andritsopoulos, J. Mol. Spectrosc. **103**, 240 (1984).
[3] T. Suzuki, Annu. Rev. Phys. Chem. **57**, 555 (2006).
[4] T. Horio, R. Spesyvtsev, and T. Suzuki, Opt. Express **21**, 22423 (2013).
[5] T. Horio, R. Spesyvtsev, and T. Suzuki, Opt. Lett. **39**, 6021 (2014).
[6] R. Spesyvtsev, T. Horio, Y.-I. Suzuki, and T. Suzuki, J. Chem. Phys. **143**, 014302 (2015).
[7] G. A. Garcia, L. Nahon, and I. Powis, Rev. Sci. Instrum. **75**, 4989 (2004).
[8] M. Hackmeyer and J. L. Whitten, J. Chem. Phys. **54**, 3739 (1971).
[9] I. C. Walker and M. H. Palmer, Chem. Phys. **153**, 169 (1991).
[10] M. P. Fülscher and B. O. Roos, Theor. Chim. Acta **87**, 403 (1994).
[11] J. E. Del Bene, J. D. Watts, and R. J. Bartlett, J. Chem. Phys. **106**, 6051 (1997).
[12] W. von Niessen, W. P. Kraemer, and G. H. F. Diercksen, Chem. Phys. **41**, 113 (1979).
[13] J. V. Ortiz and V. G. Zakrzewski, J. Chem. Phys. **105**, 2762 (1996).
[14] D. M. P. Holland, A. W. Potts, L. Karlsson, M. Stener, and P. Decleva, Chem. Phys. **390**, 25 (2011).
[15] C. Fridh, L. Åsbrink, B. Ö. Jonsson, and E. Lindholm, Int. J. Mass Spectrom. Ion Phys. **8**, 101 (1972).
[16] M. Oku, Y. Hou, X. Xing, B. Reed, H. Xu, C. Chang, C. Y. Ng, K. Nishizawa, K. Ohshimo, and T. Suzuki, J. Phys. Chem. A **112**, 2293 (2008).
[17] R. E. Turner, V. Vaida, C. A. Molini, J. O. Berg, and D. H. Parker, Chem. Phys. **28**, 47 (1978).
[18] C. F. Dion and E. R. Bernstein, J. Chem. Phys. **103**, 4907 (1995).
[19] J. K. Song, M. Tsubouchi, and T. Suzuki, J. Chem. Phys. **115**, 8810 (2001).
[20] Y.-I. Suzuki, T. Fuji, T. Horio, and T. Suzuki, J. Chem. Phys. **132**, 174302 (2010).
[21] C. Woywod, W. Domcke, A. L. Sobolewski, and H. J. Werner, J. Chem. Phys. **100**, 1400 (1994).
[22] Y. Udagawa, M. Ito, and I. Suzuka, Chem. Phys. **46**, 237 (1980).
[23] I. Yamazaki, T. Murao, T. Yamanaka, and K. Yoshihara, Faraday Discuss. **75**, 395 (1983).
[24] Y.-I. Suzuki and T. Suzuki, J. Chem. Phys. **137**, 194314 (2012).
[25] M. Staniforth, S. Daly, K. L. Reid, and I. Powis, J. Chem. Phys. **139**, 064304 (2013).
[26] T. Horio, T. Fuji, Y.-I. Suzuki, and T. Suzuki, J. Am. Chem. Soc. **131**, 10392 (2009).
[27] S. Y. Liu, Y. Ogi, T. Fuji, K. Nishizawa, T. Horio, T. Mizuno, H. Kohguchi, M. Nagasono, T. Togashi, K. Tono, M. Yabashi, Y. Senba, H. Ohashi, H. Kimura, T. Ishikawa, and T. Suzuki, Phys. Rev. A **81**, 031403 (2010).
[28] P. Zuo, T. Fuji, and T. Suzuki, Opt. Express **18**, 16183 (2010).
[29] M. Ghotbi, P. Trabs, M. Beutler, and F. Noack, Opt. Lett. **38**, 486 (2013).
[30] T. Horio, R. Spesyvtsev, K. Nagashima, R. A. Ingle, Y.-I. Suzuki, and T. Suzuki, J. Chem. Phys. **145**, 044306 (2016).